Acoustic emission monitoring for corrosion damage detection and classification

10

P. Ziehl [1], *M. ElBatanouny* [2]
[1]University of South Carolina, Columbia, SC, USA; [2]Wiss, Janney, Elstner Associates, Inc., Northbrook, IL, USA

10.1 Overview of the acoustic emission technique

Acoustic emission (AE) is the term used to define transient stress waves emitted from sudden release energy (ASTM E1316-13c, 2013) due to a deformation in the monitored material, such as crack formation or growth (Pollock, 1986; Ziehl, 2008). AE is a passive nondestructive evaluation/structural health monitoring (NDE/SHM) technique that does not need excitation or human intervention after the sensors are connected to the data acquisition system. The waveform of each AE signal (AE hit) can be used to calculate different parameters such as amplitude, duration, counts, rise time, absolute energy, and signal strength along with different frequency parameters as shown in Figure 10.1.

AE has the ability to locate cracks using triangulation. The location of each AE source event (AE signals that are detected by at least two sensors) can be determined using the arrival times of the compression waves. Assuming that the source lies in the (x,y) plane, the arrival time at the mth transducer is given by:

$$t_m = |d_m - d|/v \tag{10.1}$$

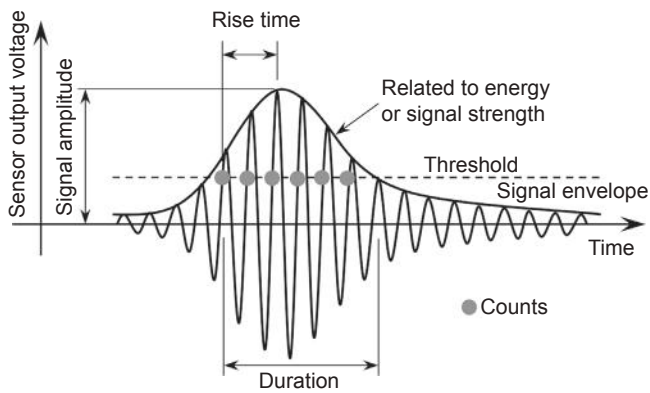

Figure 10.1 Schematic of acoustic emission waveform (ElBatanouny et al., 2014d).

Corrosion of Steel in Concrete Structures. http://dx.doi.org/10.1016/B978-1-78242-381-2.00010-9

$$t_m = \left[(x_m - x)^2 + (y_m - y)^2\right]^{1/2} \Big/ v \tag{10.2}$$

$$\Delta t_{km} = (|d_k - d| - |d_m - d|)/v \tag{10.3}$$

where v is the compression wave speed, $d = (x,y)$ is the source location, and $d_m = (x_m,y_m)$ is the location of the mth transducer. Because the absolute time of the source event is unknown, only time differences can be measured. Equations of this form are nonlinear and difficult to solve analytically, and numerical methods are generally implemented. While at least three transducers are required in order to measure two time differences and hence deduce the two unknowns *x, y* (Scruby et al., 1985), using more sensors improves source location accuracy (Miller and Mclntire, 1987). Nonlinear least-squares methods can be used to solve the equations for x and y (Scruby et al., 1985; Maji et al., 1990), and iterative procedures have been proposed by Enoki and Kishi (1988) and Ohtsu (1987), who also took into account the anisotropy of the compression wave speed in reinforced concrete (RC). The accuracy of source location in RC structures using AE has also been investigated (Grosse and Ohtsu, 2008; Shokri and Nanni, 2014). Well-established source location algorithms are usually embedded in AE data acquisition systems.

Due to the extreme sensitivity of the method, data filtering is a crucial step in AE analysis. The main source of noise in the AE data in laboratory testing is wave reflections. Duration-amplitude (D-A) filters, also known as Swansong II filters (Fowler et al., 1989), and rise time−amplitude (R-A) filters (ElBatanouny et al., 2014a) are widely used for rejection of wave reflections from AE data. These filters are usually developed through visual inspection of waveforms related to noise, and determining the relation between AE parameters for these hits. Literature indicates that crack maps can be produced with high reliability if proper data filters were used (Abdelrahman et al., 2014; ElBatanouny et al., 2014a,b).

Quantitative waveform analyses, such as source characterization (Wadley and Scrubby 1983; Kim and Sachse 1984) and moment tensor analysis (Ohtsu 1991, 1995), provide size, orientation, movement, and mode of AE sources, in addition to source location of AE events. Quantitative analyses are based on the generalized theory of AE (Ohtsu and Ono, 1984), which is based on the representation theorem of seismic sources (Aki and Richards, 1980) and models AE sources using a seismic moment tensor (Enoki and Kishi, 1988).

A simplified AE moment tensor analysis was introduced by Ohtsu (1991) using the simplified Green's function for moment tensor analysis (SiGMA) code, which has proven to be effective for analyzing fracture processes (Yuyama 2005; Ohno and Ohtsu 2010). Quantitative analyses have been applied to field geometries, such as a large concrete block or column, the corner of a rigid frame, a dam, and so forth (Yuyama, 2005). Moment tensor analysis has recently been implemented at the University of South Carolina during fatigue tests on compact tension specimens, enabling detection of crack locations and orientations. Source characterization was likewise performed to discriminate between ductile and brittle cracking mechanisms, and the results were confirmed through SEM micrographs (Hossain et al., 2012). When the

first compressive wave amplitudes are detectable and discernible at more than six observation points (AE sensors) an accurate three-dimensional source location is possible. If the specimen is comparable to a thin plate, a two-dimensional sensor placement with four sensors can be applied (Shigeishi and Ohtsu, 1992).

Moment tensor analysis is applicable even if there is access only to the outside of the structure (i.e., if all AE sensors must be placed on the outside plane). Murakami et al. (1993) reported that the analysis was successfully made in a large concrete block with all six sensors placed on the top plane. While the moment tensor approach can provide information related to damage sources, the primary limitation of this approach is the relatively dense sensor grid that must be used to obtain this information. Therefore, trade-offs exist between implementation costs and the results desired, and these must be taken into consideration for field applications.

Successful field applications of AE monitoring have been developed based on waveform analysis combined with damage rates that are based on parameters of the received waveform such as signal strength and energy. Much of the earlier work in AE was based on empirical observations of damage and large datasets, and trend analysis was utilized to track and quantify trends in AE data rates. This approach was highly successful in the fiber-reinforced polymer pressure vessel industry and also for qualification of railroad tank cars (Fowler et al., 1989). More recently, formalized pattern recognition techniques have been introduced to characterize the structure and to determine natural "signatures" in AE datasets (Marec et al., 2008; Gutkin et al., 2011; Li et al., 2012; Sause et al., 2012). Such techniques have evolved toward machine learning and data mining, which have been used for classification, regression, and prediction. Current investigations are implementing data mining tools for hypothesis searching, rule extraction, and decision making (e.g., Bhat et al., 2003; Olivera and Marques 2008; Qian et al., 2009; Omkar and Karanth 2008). Recently, Mejia (2012) addressed a common and important pattern recognition problem in AE: the presence of unwanted signals (or "noise") in AE datasets. The study designed and implemented a data mining scheme that enhanced the quality of AE datasets. The scheme was able to produce characterization rules for both unwanted and meaningful signals, showing that rule extraction using this technique could lead to the finding of general AE "signatures" for particular damage mechanisms.

10.2 Mechanism of corrosion detection using AE

Corrosion of reinforcement is a major cause for deterioration of RC structures in coastal areas or areas where deicing salts are used. In spite of the natural protection concrete provides for the steel reinforcement to resist corrosion due to formation of protecting passive oxide film around the steel as a result of the high alkalinity of concrete; however, chlorides can infiltrate through concrete cracks to break the passive film and initiate corrosion in reinforcing steel.

Chloride-induced corrosion reduces the mechanical strength of steel reinforcement and corrosion product exerts stress into the concrete structure that produces cracks that deteriorate the steel−concrete bond, which directly affects serviceability performance.

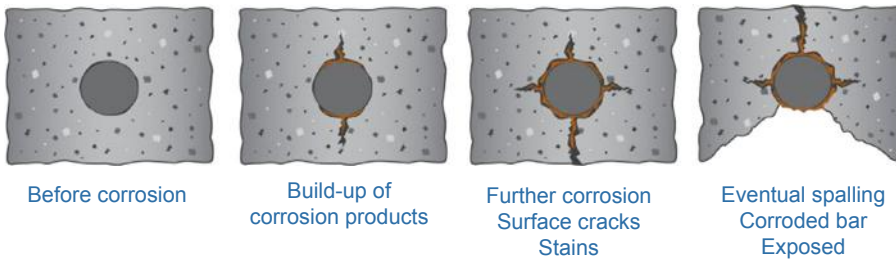

Figure 10.2 Corrosion process in concrete (http://concrete-forum.com/).

When steel starts to corrode, a gradual decrease of its diameter is produced, together with the generation of an oxide with a volume 6 to 10 times higher than that of steel (Li et al., 1998). The corrosion process is then accelerated by the presence of cracks, which increases the rate of chloride infiltration. Corrosion affects the durability of concrete structures and decreases its service life by: (1) reducing the cross-sectional area of the steel strands minimizing their ductility and increasing stress concentrations at the reinforcement interface (Yoon et al., 2000) and (2) degrading the integrity of the surrounding concrete (Jaffer and Hanson, 2009). Figure 10.2 shows a schematic of the corrosion process in concrete.

The mechanisms that enable correlation between AE data and corrosion intensity are: (1) accumulation of chlorides and breakdown of the passive film (Perrin et al., 2010; Prateepasen and Jirarungsatian, 2011) and (2) the microcracking of the concrete that occurs due to the expansive nature of the corrosion products (ElBatanouny et al., 2011, 2014c; Mangual et al., 2013a,b). The primary advantage of AE monitoring is its unique ability to detect and quantify the microcracking process as it occurs, making it an extremely sensitive monitoring method. Later stages of corrosion damage, such as visible surface cracking, are also easily detected and quantified.

10.3 Case studies for corrosion detection using AE

The use of AE to detect corrosion damage in RC started in the 1980s (Weng et al. 1982; Abdelrahman, 2013). However, most of the studies focused only on passively reinforced rather than prestressed concrete (PC). The main focus of earlier studies was to investigate the ability of AE to detect corrosion initiation. Literature indicates that AE parameters such as number of AE hits and/or events have the ability to detect corrosion as well as changes in the rate of the corrosion process (Li et al., 1998; Zdunek et al., 1995; Idrissi and Limam, 2003).

Figure 10.3 shows the results of AE events and current versus time (Li et al., 1998). This figure indicates the ability of AE to detect microcracking associated with corrosion damage. In addition, AE activity increased prior to the increase in galvanic current, which illustrates the ability of AE to detect corrosion damage earlier than can be achieved using electrochemical measurements.

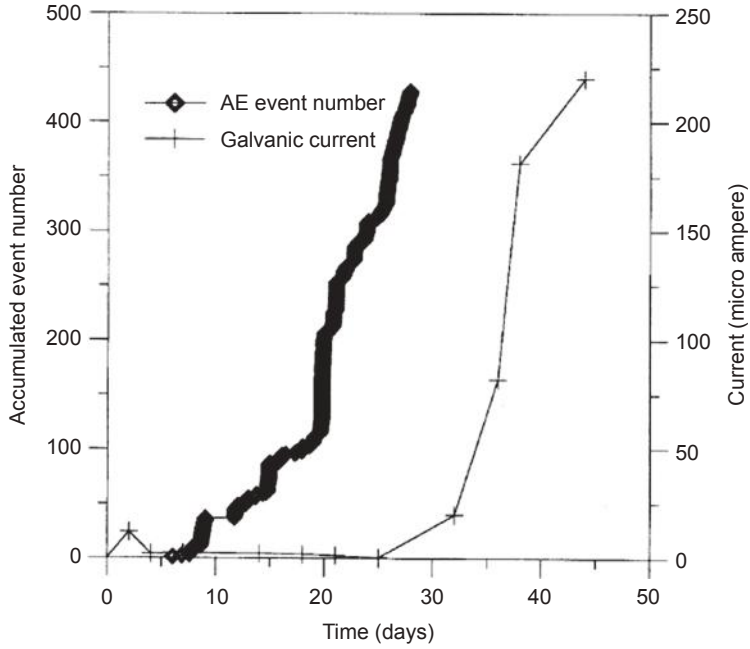

Figure 10.3 AE versus galvanic current readings (Li et al., 1998).

Recent studies also have investigated the use of AE-based condition assessments such as SiGMA, R-A value, and *b*-value (Farid Uddin et al., 2004; Ohtsu and Tomoda, 2008). Figure 10.4 shows the results of *b*-value versus time during an accelerated corrosion test using wet/dry cycles on a small scale specimen (Ohtsu and Tomoda, 2008). During this test, half-cell potential (HCP) measurements started decreasing at

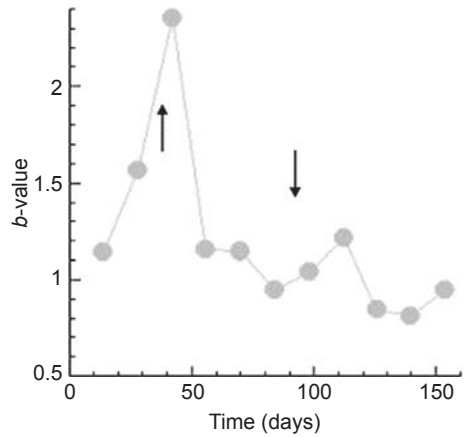

Figure 10.4 Variation of *b*-values in cyclic wet/dry test (Ohtsu and Tomoda, 2008).

approximately 100 days. A drop in the *b*-value was observed at the same time, indicating that corrosion damage is occurring. The rise in the *b*-value at approximately 40 days of testing was attributed to corrosion initiation, as the chloride concentration exceeded the threshold at this time.

10.4 Corrosion classification using AE

Most of the earlier studies focused on RC specimens and showed that AE can detect corrosion damage, but they did not directly relate AE activity to the rate of corrosion and in determining the extent of corrosion. Although the mechanism of corrosion activity in RC and PC is similar, the manufacturing process and shape of prestressing strands facilitates corrosion initiation at a lower chloride concentration as compared with steel rebars (Moser et al., 2011). This section summarizes recent efforts at the University of South Carolina for corrosion detection and classification of prestressing strands in PC and post-tensioned concrete (PT) specimens with different scales and durations of corrosion exposure. In these studies, 1/2 in. (12.7 mm) seven-wire low-relaxation prestressing strands were used in all specimens. AE R6i sensors (peak resonance at approximately 55 kHz, with integral 40 dB_{AE} (referred to as dB for simplicity) preamplification) were used to monitor corrosion in all the studies. It is noted that all the AE data shown is filtered. The main filters used are D-A filters, which are based on inspection of AE signals to differentiate noise from genuine AE data. The limits used in the D-A filters from ElBatanouny et al. (2014c) are shown in Table 10.1. For more information regarding the filtration techniques, please refer to the referenced manuscripts (ElBatanouny et al., 2014c; Mangual et al., 2013a,b).

10.4.1 Small-scale specimens

A total of 20 specimens were tested under an accelerated corrosion test setup. The specimens were reinforced with an embedded 1/2-inch-diameter prestressing strand;

Table 10.1 AE duration-amplitude data filter (ElBatanouny et al., 2014c)

Rejection limits		Rejection limits		Rejection limits	
Amp (dB)	**Dur (μs)**	**Amp (dB)**	**Dur (μs)**	**Amp (dB)**	**Dur (μs)**
40–42	>400	50–52	>1500	60–65	>4500
42–44	>600	52–54	>2000	65–70	>6500
44–46	>800	54–56	>2500	70–75	>7500
46–48	>1000	56–58	>3000	75–80	>9000
48–50	>1200	58–60	>3500	90–100	>10,000

dimensions of each specimen were 4.5 in. × 4.5 in. × 20 in. (114 mm × 114 mm × 1270 mm). The test matrix included 11 precracked specimens and 9 pristine specimens to evaluate the effect of cracks on AE attenuation. Specimens were immersed in a tank filled with a 3% NaCl solution at room temperature to a level 0.25 in. (7 mm) below the reinforcing strand. A copper plate with the same length of the specimens was placed below each specimen to serve as the cathode.

Accelerating the corrosion process was established by forming a galvanic cell using a rectifier to impress a direct external current to the specimens. The current that flows between the dissimilar metals controls the degree of corrosion activity in the cell. The rectifier was connected between the copper plate (cathode) and the prestressing strand (anode). Figure 10.5 shows a diagram of the corrosion cell for a single cracked specimen placed in the test vessel (Mangual et al., 2013a).

The results showed that stresses induced by volume expansion resulted in dense AE that was correlated to the onset of corrosion and nucleation of cracks as shown in Figure 10.6. Comparing AE data with electrochemical HCP measurements showed that the cumulative signal strength (CSS) relates well with potential variations as

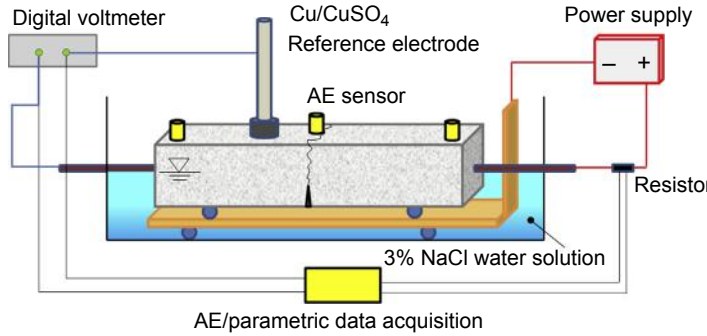

Figure 10.5 Schematic of the accelerated corrosion setup (Mangual et al., 2013a).

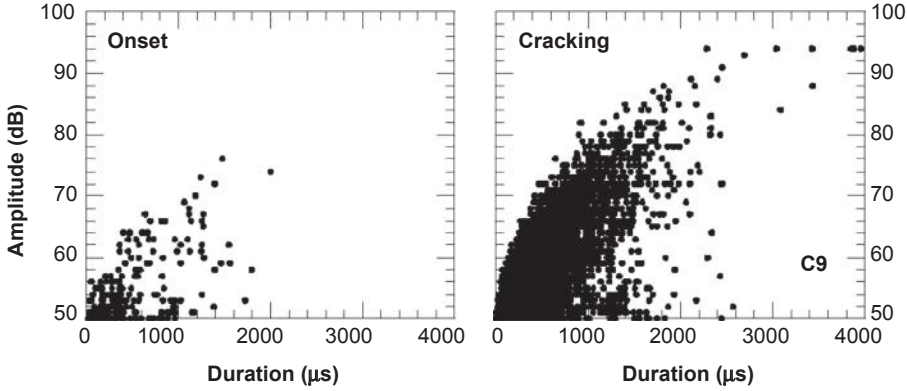

Figure 10.6 Amplitude (dB) versus duration (µs) plot (Mangual et al., 2013a).

shown in Figure 10.7. It also allowed discrimination between different corrosion stages. The magnitude of the slope in the CSS versus time curve was able to portray the depassivation process and onset of corrosion as corroborated by HCP. This shows that AE is capable of detecting and discriminating between early corrosion stages while mimicking the behavior of resistivity changes in the concrete.

Source location based on AE data enabled the accurate detection of events as a result of passivity breakdown along the reinforcement and debonding (Mangual et al., 2013a). Figure 10.8 shows the source location results for a precracked specimen. As seen in the figure, most of the AE activity concentrated near to the crack where corrosion is predicted to take place as a result of chloride accessibility in this region (no AE activity was detected at the exact crack location, as it is already formed). At the conclusion of the test, the specimens were taken apart, and the strand was removed for visual inspection of corrosion. The strand was then cleaned and reweighed to measure the steel mass loss as detailed in Mangual et al., (2013a). As shown in Figure 10.9, heavy corrosion damage, in terms of formation of longitudinal and tangential cracks, was observed in some specimens.

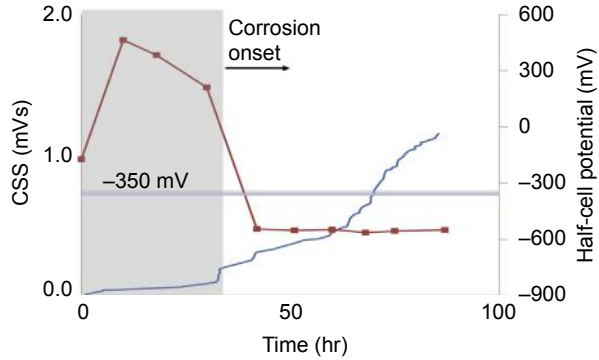

Figure 10.7 CSS and HCP versus time.

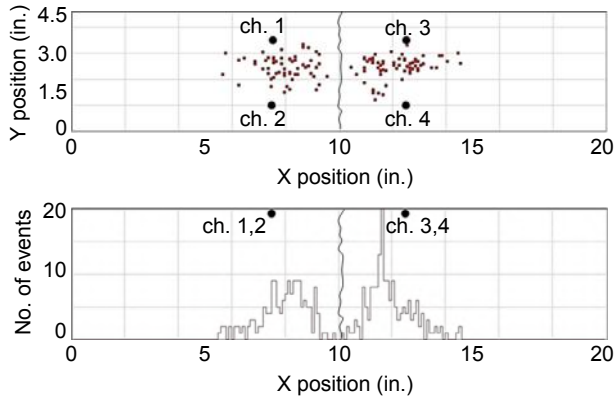

Figure 10.8 Source location and number of events for a precracked specimen.

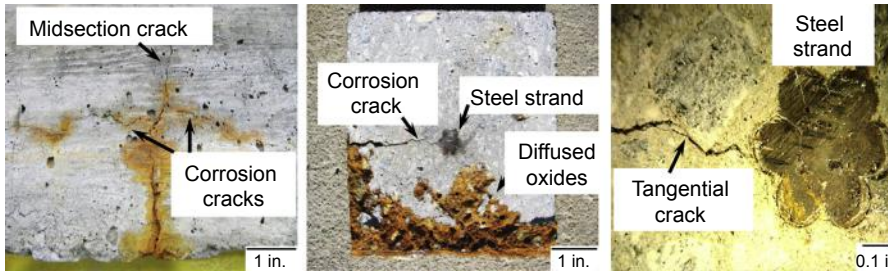

Figure 10.9 Corrosion damage in steel and concrete.

ElBatanouny et al. (2011) proposed that AE intensity analysis can be used to classify corrosion damage. The method was first proposed by Fowler et al. (1989) to quantify damage in fiber reinforced polymers (FRP) vessels and tanks by calculating two parameters: historic index, $H(t)$, and severity, S_r. Historic index is a form of trend analysis that measures the rate of change in the CSS, while severity is the average of a certain number of hits (50 hits) with the highest signal strength. The increase in these parameters can be related to accumulation of damage. Historic index and severity can be calculated using Eqns (10.4) and (10.5), where N is number of hits up to a time (t), S_{oi} is the signal strength of the ith event, and K is an empirically derived factor that varies with the number of hits. In this study, the value of K was selected to be: (a) N/A if $N \leq 50$; (b) $K = N - 30$ if $51 \leq N \leq 200$; (c) $K = 0.85N$ if $201 \leq N \leq 500$; and (d) $K = N - 75$ if $N \geq 501$.

$$H(t) = \frac{N}{N-K} \frac{\sum_{i=k+1}^{N} S_{oi}}{\sum_{i=1}^{N} S_{oi}} \tag{10.4}$$

$$S_r = \frac{1}{50} \sum_{i=1}^{i=50} S_{oi} \tag{10.5}$$

Intensity analysis results were correlated with HCP measurements and measured sectional mass loss, yielding two AE-based corrosion classification charts for precracked and uncracked specimens as shown in Figure 10.10. For precracked specimens, the chart divides the corrosion damage into four categories as illustrated in Mangual et al. (2013a) as follows: (1) No damage: at this level the steel is still in the passive condition and no corrosion damage occurred, (2) Depassivation: at this level corrosion has just initiated with sectional mass loss less than 15%, (3) Cracking: refers to the level at which cracks due to corrosion started to form and the sectional mass loss is less than 21%, and (4) Severe damage: more cracks form and the sectional mass loss exceeds 21%. For pristine specimens, specimens in which depassivation was absent laid in region A of the intensity analysis grading chart, whereas depassivated specimens lay in the B region (Mangual et al., 2013b). These charts enable early detection of corrosion and classification of corrosion damage. Such charts also could extend

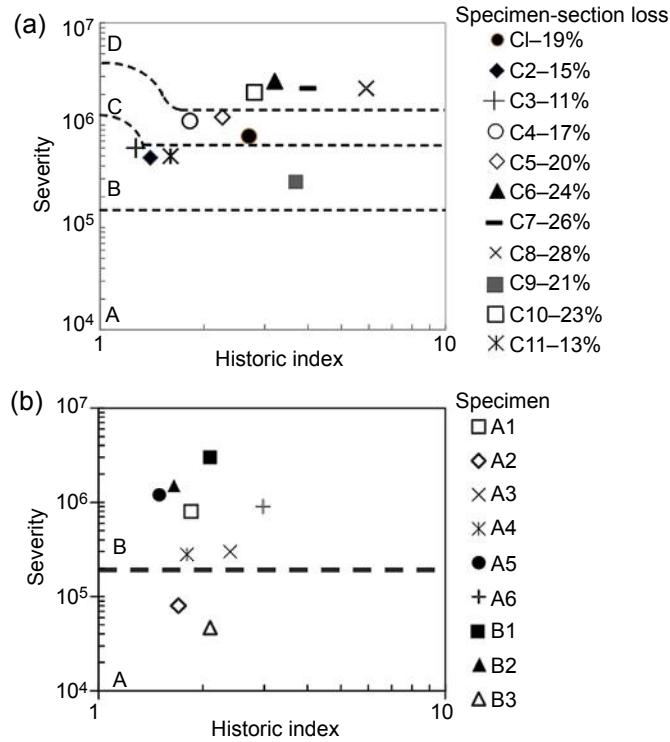

Figure 10.10 AE-based corrosion classification charts for: (a) precracked specimens and (b) pristine specimens (Mangual et al., 2013a,b).

the use of AE to personnel who are less acquainted with methods of performing damage evaluation, without the need to send the collected data to an AE specialist. It is noted that these figures include uncertainties associated with AE monitoring that should be studied and quantified in future studies.

10.4.2 Medium-scale specimens

Long-term corrosion tests were performed on medium-scale PC beams to provide better representation of actual environments for corrosion. The corrosion was accelerated using three-day-wet/four-day-dry cycles with a 3% NaCl solution as shown in Figure 10.11. Each beam was reinforced with two 1/2 in. (12.7 mm) prestressing strands located in the compression zone and measured 16 ft 4 in. in length (4.98 m). The beams were T-shaped with a total height of 15 in. (380 mm), a web thickness of 6 in. (150 mm), and a flange width and depth of 24 in. (610 mm) and 3 in. (75 mm), respectively. The test included three specimens, where two were precracked to 0.016 in. (0.4 mm), specimen CC-0.4; and 0.032 in. (0.8 mm), specimen CC-0.8; while the last specimen was pristine. The specimens were continuously monitored by AE for 140 days. No corrosion damage was detected in the pristine specimen

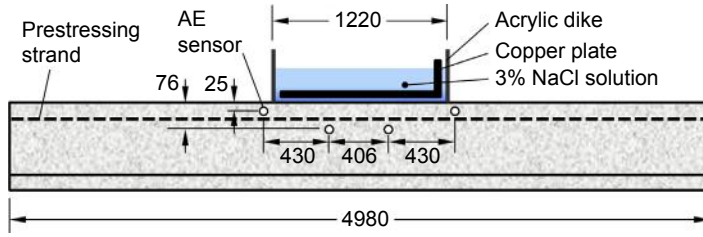

Figure 10.11 Corrosion test setup and AE sensor layout (in mm; 1 in. = 25.4 mm) (ElBatanouny et al., 2014c).

from any method due to the limited ability of chlorides to penetrate through concrete subjected to prestressing force.

The results of the precracked specimens showed that the AE parameter CSS is able to detect corrosion with a higher sensitivity than HCP. As shown in Figure 10.12, HCP for specimen CC-0.8 showed that corrosion initiated within the first week of testing agreed with CSS results that showed a high rate of corrosion activity. For specimen CC-0.4, HCP results only approached the corrosion threshold toward the

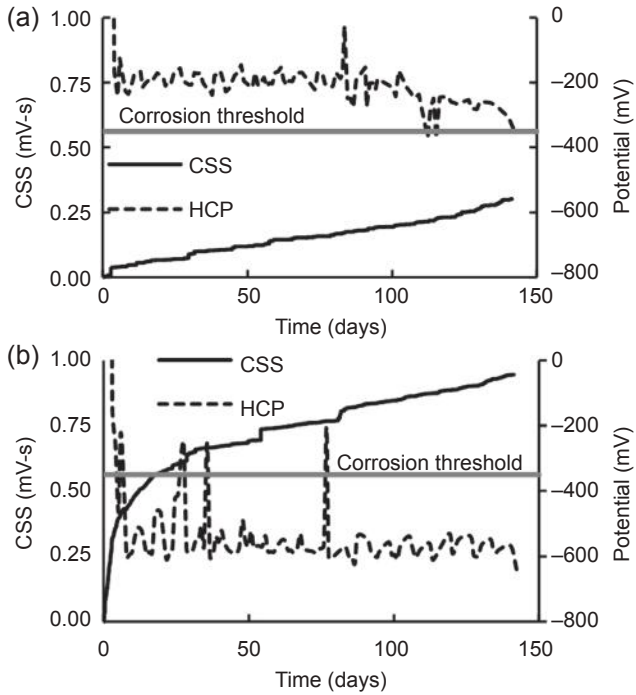

Figure 10.12 CSS and HCP versus time. (a) Specimen precracked crack width (a) 0.016 in. (0.4 mm), specimen CC-0.4 and (b) 0.032 in. (0.8 mm), specimen CC-0.8 (ElBatanouny et al., 2014c).

end of the test while AE was showing a steady increase in the AE activity, illustrating that corrosion is occurring. To further investigate the corrosion activity, linear polarization resistance (LPR) measurements were also taken to calculate the corrosion rate. Based on Andrade et al. (1990) classification, LPR results showed that CC-0.4 had a moderate corrosion rate, while CC-0.8 had a high corrosion rate. This agrees with the AE results, where the rate of AE activity for CC-0.8 was higher than that of CC-0.4. Visual inspection of damaged prestressing strands showed clear evidence of pitting (localized) corrosion in both specimens as shown in Figure 10.13. This corrosion type leads to a significant reduction in the residual capacity of the specimens. Crack width is a significant factor in the formation and intensity of pitting in terms of pit depth. Load testing of the beams at the conclusion of the test showed a reduction in the capacity of the beams where corrosion was detected by AE, as compared with the pristine specimen where no corrosion was detected. This indicated that AE has the ability to detect corrosion before a reduction in the strength of the structure occurs. Therefore, adapting this method for real-time corrosion monitoring can reduce, if not eliminate, the risk of sudden failure as a result of corrosion damage (ElBatanouny et al., 2014c).

Intensity analysis was performed on the cracked specimens using the limits set in the small-scale specimens study as shown in Figure 10.14. The results showed that AE intensity analysis can enable the detection and classification of corrosion damage. This is true for small- and medium-scale specimens, illustrating that the method may be independent of specimen size and duration of exposure. These results were also compared with LPR results and had a good agreement.

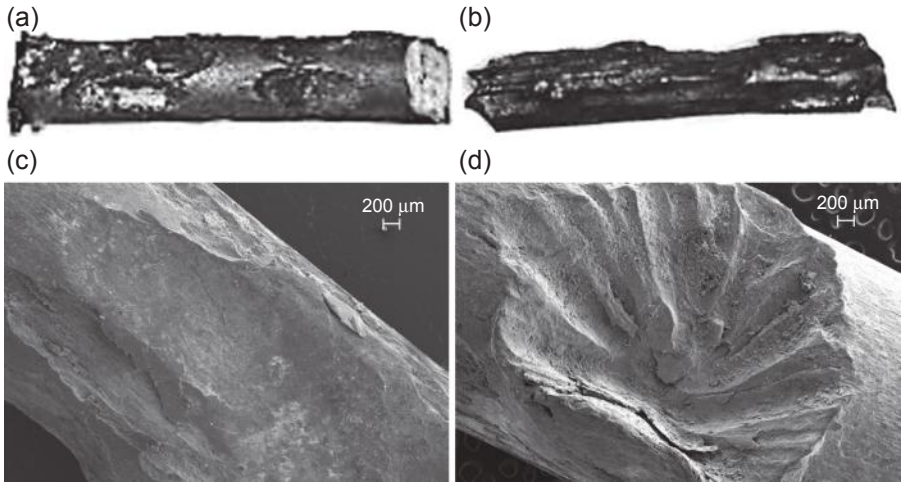

Figure 10.13 Photographs showing pitting corrosion: (a, b) specimens CC-0.4 and CC-0.8, respectively, and (c, d) SEM micrographs of specimens CC-0.4 and CC-0.8, respectively (1 in. = 25.4 mm) (ElBatanouny et al., 2014c).

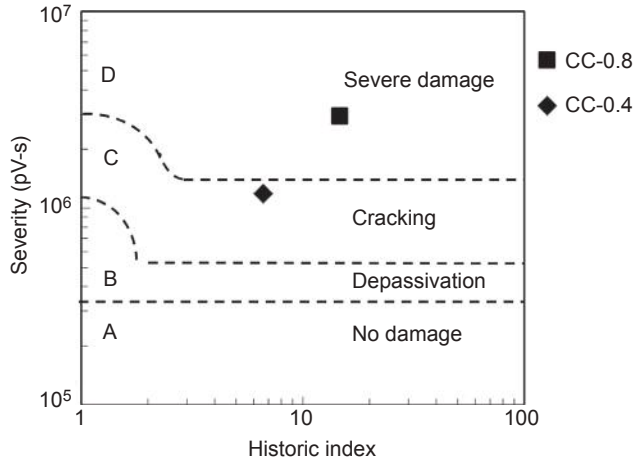

Figure 10.14 Corrosion intensity analysis results for cracked specimens (ElBatanouny et al., 2014c).

10.5 Special considerations and potential applications in the field

AE is a nonintrusive method that has the ability to detect damaged areas through source triangulation. The high sensitivity of the method enables it to perform global assessment of the structure. However, effective filtering protocols are needed for field applications to reject noise related to environmental containments such as rain, hail, and wind with debris.

The method is currently deployable in elements such as piles and foundations. For superstructures, a method to separate AE data from corrosion and that from other sources such as service loading should be developed. More studies should be conducted on the applicability of the developed charts for field applications. Uncertainties related to noise rejection, AE wave speed, and signal attenuation in the field should also be investigated (ElBatanouny et al., 2014d).

10.6 Special considerations for wireless sensing

AE systems have been steadily developing over the past decades to become affordable and deployable. Currently, a self-powered wireless AE system is commercially available in the United States through Mistras Group, Inc. This makes AE suitable for remote/real-time/rapid inspection of massive structures using a minimal number of sensors. The authors of this chapter successfully implemented AE wireless systems in a previous project with the Savannah River National Laboratory, where

AE sensors were embedded in a mesoscale test bed to monitor cracks in grout used for in situ decommissioning of nuclear structures (Ziehl et al., 2012; ElBatanouny et al., 2012).

The wireless AE system "smart node" reduces the data transferred wirelessly by sending the waveform parameters without including the waveforms. The waveforms are saved on an SD card that is attached to the node for more detailed signal processing. This data-reduction technique enables the system to process and send data wirelessly in real-time and reduces the possibility of data loss due to insufficient buffer. However, the capacity of data collection of the wireless system is less than that of wired systems. Therefore, future efforts should focus on comparing AE data collected from wireless AE systems with those of wired AE systems. Since all damage-evaluation techniques proposed are based on wired systems, a probabilistic analysis should be conducted to evaluate and modify damage assessment limits for wireless systems.

10.7 Summary

The feasibility of AE to detect corrosion was evaluated by comparing AE results with electrochemical methods, sectional mass loss, and visual evidence of corrosion damage. AE parameters such as cumulated events and signal strength were found to detect the initiation of corrosion prior to electrochemical measurements. The method can be effectively used in places where there is no provision for electrochemical measurements. AE-based intensity analysis charts can enable the detection and classification of corrosion damage using empirical limits for corrosion levels. This chart classifies corrosion damage in specimens with different sizes and exposure times showing that it may be independent of size and duration.

Unlike some electrochemical techniques, the proposed AE corrosion classification charts have the ability to detect and quantify corrosion damage at early stages. This enables the development of AE into a damage quantification tool for maintenance prioritization because significant damage (such as macrocracking and spalling) is not required for detection. The proposed chart can also be used to estimate safe remaining service life as it is linked to cross-sectional mass loss results. However, the uncertainties associated with the relation between AE and mass loss should be quantified prior to full implementation.

Acknowledgments

Portions of this work were published in the Precast/Prestressed Concrete Institute Convention-National Bridge Conference Proceedings (PCI-NBC), 2014 held in Washington, DC in a paper titled "Review of Acoustic Emission Corrosion Monitoring of Prestressed Concrete Bridges."